

Cell Deformation Passing through Slit between Micro-Machined Surfaces *in Vitro*: Comparison among Cell Types

Shigehiro HASHIMOTO, Keisuke KAKISHIMA, Yusuke TAKAHASHI

Biomedical Engineering, Department of Mechanical Engineering,
Kogakuin University, Tokyo, 163-8677, Japan
<http://www.mech.kogakuin.ac.jp/labs/bio/>

ABSTRACT

Deformation of cell passing through the slit between micro-machined surfaces has been observed *in vitro*. At the middle part of the flow channel, the slit (0.8 mm width, and 0.01 mm height) has been made between the transparent polydimethylsiloxane plate and glass plate, of which surfaces are micro-machined by photolithography technique. Four kinds of cells were used in the test: C2C12 (mouse myoblast cells), Hepa1-6 (mouse hepatoma cells), L929 (fibroblast connective tissue of mouse), and Neuro-2a (mouse neural crest-derived cell line). The suspension of each kind of cells was injected to the slits. The deformation of each cell passing through the micro slit was observed with an inverted phase-contrast microscope. The experimental results show that each cell deforms to the flat disk and passes through the micro slit of 0.01 mm height. Both the projected area and the passing velocity of each cell in the slit were measured. The passing velocity of each cell tends to decrease with the higher deformation. At some cells of C2C12, the velocity in the slit is higher than that before the slit even at the higher deformation ratio. The designed slit between micro-machined surfaces has capability to sort the deformability of cells.

Keywords: Biomedical Engineering, C2C12, Hepa1-6, L929, Neuro-2a, Photolithography and Micro-slit.

1. INTRODUCTION

The deformability of the biological cell plays an important role *in vivo*. A red blood cell, for example, has high flexibility. The elasticity of the membrane [1], and fatigue [2] were evaluated in the previous studies. The aging effect on deformability [3] and the sublethal damage [4] were also detected in the shear flow in the previous studies. It also passes through micro-circulation, of which the dimension is smaller than the diameter of the red blood cell. After circulation through the blood vessels for days, the red blood cell is trapped in the micro-circulation systems.

Several systems sort cells according to the deformability *in vivo*. One of the systems, which trap red blood cells, is a spleen. The spleen has special morphology at the blood flow path to sort injured red blood cells [5]. A slit is one of the systems, which sorts biological cells *in vivo*. The sorting at the slit depends on the deformability of each cell. Some cells are able to pass through a very narrow slit.

A photolithography technique enables manufacturing micro grooves [6] or micro structures [7] in the flow-channel for cell tests *in vitro*. Several micro-fabrication processes have been designed to simulate morphology of the microcirculation [8]. The technique also has been applied to handle cells in diagnostics *in vitro* [9]. The photolithography technique can be applied to make a micro slit. The slit between micro cylinders was made to sort cells in the previous study [10]. The deformation of the depth direction between cylinders, however, cannot be observed by the conventional optical microscope. To observe the deformed cell at the direction perpendicular to the walls of the slit, another type of the slit is designed with the combination of micro ridges in the previous study [11].

In the present study, a micro slit has been fabricated between micro-machined surfaces by the photolithography technique, and deformation of a biological cell passing through the micro slit has been compared among cell types experimentally *in vitro*.

2. METHODS

Micro Slit

The slit has been designed between a transparent polydimethylsiloxane (PDMS) plate and a borosilicate glass (Tempax) plate (Fig. 1). The upper plate of PDMS has a rectangular ridge of 0.05 mm height, 0.10 mm width, and 2 mm length. The lower plate of glass has a rectangular groove of 0.010 mm depth (H), 2 mm width, and 20 mm length, which has a narrow part of 0.8 mm width. These plates make contact to make slits (width (W) of 0.8 mm, length (L) of 0.1 mm and height (H) of 0.010 mm) between them.

Photomask for Upper Plate

The glass plate of 0.2 mm thick was used for the base of the mask (Fig. 2). Before the vapor deposition of titanium, the surface of the glass plate was hydrophilized by the oxygen (30 cm³/min, 0.1 Pa) plasma ashing for five minutes at 100 W by the reactive ion etching system (FA-1, Samco Inc., Kyoto). Titanium was coated on the surface with 150 nm thick in the electron beam vapor deposition apparatus (JBS-Z0501EVC, JEOL Ltd., Japan). The positive photoresist material of OFPR-800LB was coated on the titanium at the plate at 7000 rpm for 60 s with a spin coater. The photoresist was baked on the heated plate at 368 K for five minutes. The pattern was drawn on the mask with a laser drawing system

(DDB-201K-KH, Neoark Corporation, Hachioji, Japan). The pattern was baked on the heated plate at 368 K for five minutes. The photoresist was developed with NMD-3 for 5 minutes. The plate was rinsed by the ultrapure water, and dried by the spin-dryer. The titanium coating plate was etched with the plasma gas (SF₆, Ar) using RIE-10NR (Samco International, Kyoto, Japan). The residual OFPR-800LB on the surface was exfoliated by acetone.

Mold for Upper Plate

A glass plate (38 mm × 26 mm × 1 mm: Matsunami Glass Ind., Ltd., Osaka, Japan) is used for a surface mold for the upper disk. The plate was cleaned by an ultrasonic cleaner with alkaline solution, and rinsed by the ultrapure water. The surface of the glass plate was hydrophilized by the oxygen (30 cm³/min, 0.1 Pa) plasma ashing for five minutes at 100 W by the reactive ion etching system (FA-1). The negative photoresist material of high viscosity (SU8-10: Micro Chem Corp., MA, USA) was coated on the glass plate at 1000 rpm for 30 s with the spin coater. After the photoresist was baked on the heated plate at 338 K for two minutes, the plate was baked on the heated plate at 368 K for seven minutes. SU8-10 was coated on the plate at 1000 rpm for 30 s with the spin coater again. After the photoresist was prebaked on the heated plate at 338 K for five minutes, the plate was baked on the heated plate at 368 K for one hour. The photomask was mounted on the surface of SU8-10, and the photoresist was exposed to the UV light through the mask in the mask aligner (M-1S, Mikasa Co. Ltd., Japan) at 15 mW/cm² for 20 s. After the photoresist was prebaked on the heated plate at 338 K for one minute, the plate was baked on the heated plate at 368 K for five minutes. The photoresist was developed with SU-8 developer (Nippon Kayaku Co., Ltd, Tokyo, Japan). The glass surface with the micro pattern was rinsed with IPA (2-propanol, Wako Pure Chemical Industries, Ltd.) for five minutes, and with the ultrapure water. The plate was dried by the spin-dryer. The plate was baked on the heated plate at 368 K for three minutes.

Upper Plate

After the mold of the glass plate was enclosed with a peripheral wall of polyimide tape, PDMS (Sylgard 184 Silicone Elastomer Base, Dow Corning Corporation) was poured together with the curing agent (Dow Corning Corporation) on the mold (Fig. 3). The volume ratio of curing agent is ten percent of PDMS. After degassing, PDMS was baked at 373 K for one hour in an oven (DX401, Yamato Scientific Co., Ltd, Tokyo, Japan). The baked plate of PDMS is exfoliated from the mold. Two holes of 8 mm diameter were machined with a punching tool at the upper disk to make the inlet and the outlet for the flow channel (Fig. 5).

Photomask for Lower Plate

The glass plate of 0.2 mm thick was used for the base of the mask. Before the vapor deposition of titanium, the surface of the glass plate was hydrophilized by the oxygen (30 cm³/min, 0.1 Pa) plasma ashing for five minutes at 100 W by the reactive ion etching system (FA-1). Titanium was coated on the surface with 150 nm thick in the electron beam vapor deposition apparatus. The part of Titanium coating was covered with the polyimide tape to make the flow channel of 2 mm width (narrow part: 0.8 mm width) × 20 mm length. The titanium coating disk was etched with the plasma gas (SF₆, Ar) using RIE-10NR. After the etching, the polyimide tape was exfoliated.

Lower Plate

A glass plate (Fig. 4) was cleaned by an ultrasonic cleaner with alkaline solution, and rinsed by the ultrapure water. The surface of the glass plate was hydrophilized by the oxygen (30 cm³/min, 0.1 Pa) plasma ashing for five minutes at 100 W by the reactive ion etching system (FA-1). The negative photoresist material of high viscosity (SU8-10) was coated on the glass plate at 2000 rpm for 30 s with the spin coater. After the photoresist was baked on the heated plate at 338 K for three minutes, the plate was baked on the heated plate at 368 K for seven minutes. The photomask was mounted on the surface of SU8-10, and the photoresist was exposed to the UV light through the mask in the mask aligner (M-1S) at 15 mW/cm² for 20 s. After the photoresist was prebaked on the heated plate at 338 K for one minute, the plate was baked on the heated plate at 368 K for five minutes. The photoresist was developed with SU-8 developer for three minutes. The glass surface was rinsed with IPA for two minutes, and with the ultrapure water. The plate was dried by the spin-dryer.

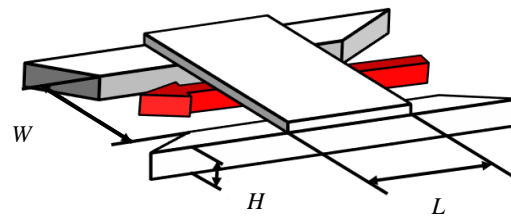


Fig. 1: Microslit.

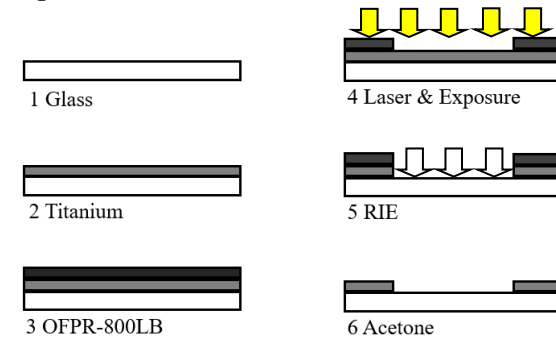


Fig. 2: Photolithography process of mask.

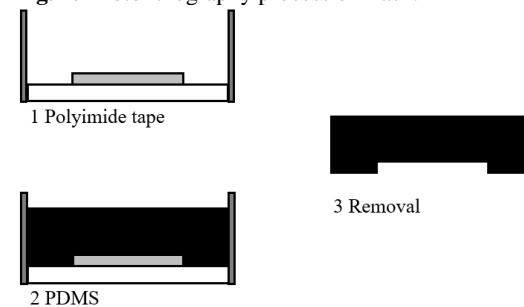


Fig. 3: Upper plate of PDMS.

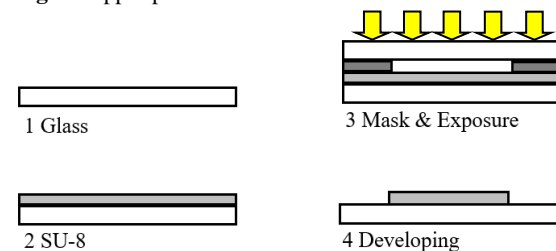


Fig. 4: Lower plate of glass.

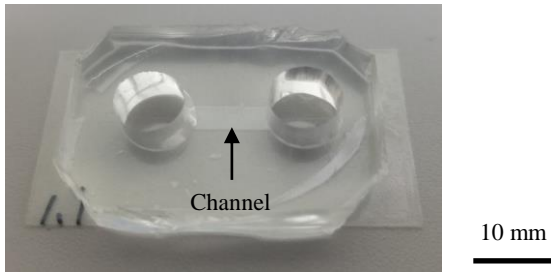


Fig. 5: Flow channel device : diameter of each hole is 8 mm.

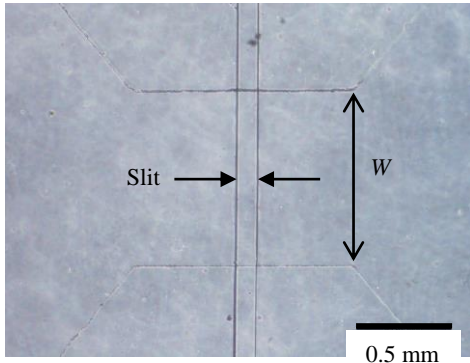


Fig. 6: Micro slit in flow channel.

Flow Channel

The upper plate of PDMS was rinsed with IPA, and with the ultrapure water. The plate was dried by the spin-dryer. The surface of the PDMS plate was hydrophilized by the oxygen (30 cm³/min, 0.1 Pa) plasma ashing for thirty seconds at 50 W by the reactive ion etching system (FA-1). The plate was rinsed with APTES (Aminopropyl-triethoxysilane) for five minutes, and with the ultrapure water. The plate was dried in the oven at 338 K for three minutes. The upper plate of PDMS was adhered on the lower plate of SU8-10 to make the slit (Figs. 5 & 6), and was baked on the heated plate at 338 K for five minutes.

Flow Test

Four kinds of cells (passage < 10) were used in the flow test: C2C12 (mouse myoblast cell line originated with cross-striated muscle of C3H mouse), Hepa1-6 (mouse hepatoma cell line of C57L mouse), L929 (fibroblast connective tissue of C3H mouse), and Neuro-2a (a mouse neural crest-derived cell line). D-MEM (Dulbecco's Modified Eagle's Medium) containing 10% FBS (decomplemented fetal bovine serum) and 1% penicillin/ streptomycin (GIBCO, Life Technologies Japan Ltd., Tokyo, Japan) was used for the medium.

The cells were exfoliated from the bottom of the culture dish with trypsin, and suspended in the culture medium. The inner surface of the flow channel was hydrophilized by the oxygen (30 cm³/min, 0.1 Pa) plasma ashing for thirty seconds at 50 W by the reactive ion etching system (FA-1). After the bovine serum albumin solution was prefilled in the flow channel, the suspension (250 μl) of the cells was poured at the inlet (8 mm diameter) of the flow channel (Fig. 7). The suspension flows by the pressure head of 5 mm, which makes the pressure difference of 49 Pa between the inlet and the outlet. The behavior of cells near the slit was observed with an inverted

phase-contrast microscope (IX71, Olympus Co., Ltd., Tokyo) at 298 K (Fig. 8).

The microscopic movie images of thirty frames per second at the shutter speed of 1/2000 s were recorded by the camera (DSC-RX100M4, Sony Corporation, Tokyo, Japan). At the images, the outline of each cell was traced with "Image J", and the projected area (A) was calculated (Fig. 9). The deformation ratio (Ra) was calculated at each cell by Eq. 1.

$$Ra = (A_2 - A_1) / A_1 \quad (1)$$

In Eq. 1, A_1 is the area before the slit, and A_2 is the area in the slit.

The velocity of the cell passing through the slit (v) was calculated at the movie by "Kinovea" (Fig. 10). Most of cells pass through the slit in a few seconds, and Data of clogging cell in the slit are not included in the following figures.

The velocity ratio (Rv) was calculated at each cell by Eq. 2.

$$Rv = (v_2 - v_1) / v_1 \quad (2)$$

In Eq. 2, v_1 is the velocity before the slit, and v_2 is the velocity in the slit.

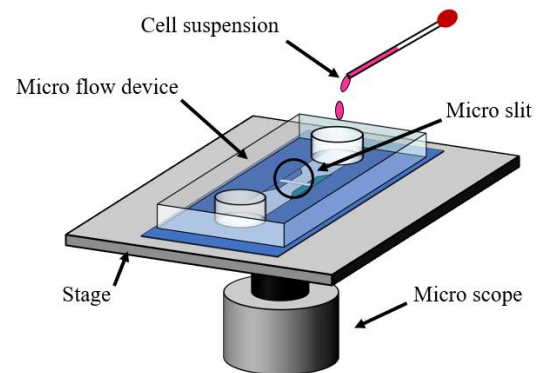


Fig. 7: Flow test.

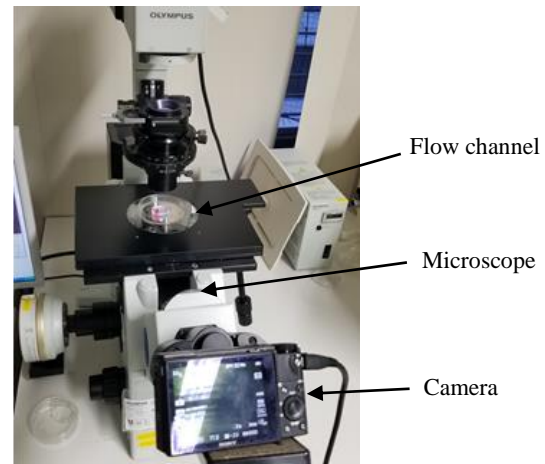


Fig. 8: Experimental system.

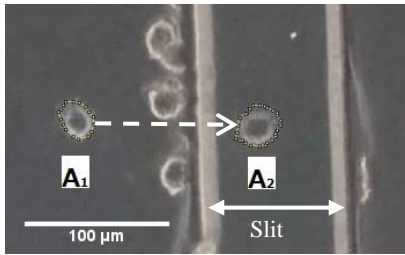


Fig. 9: Tracings of projected area of each cell: area before slit (A_1), in slit (A_2): flow from left to right.

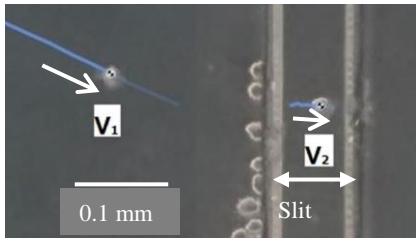


Fig. 10: Tracings of movement of each cell: velocity before slit (v_1), in slit (v_2): flow from left to right.

3. RESULTS

Fig. 11 exemplifies cell passing through the slit. A cell approaches to the slit (A), enters the slit (B), is passing through the slit (C), and leaves from the slit (D).

Figs. 12–15 show the projected area (Fig. 12a, Fig. 13a, Fig. 14a, and Fig. 15a) and the velocity (Fig. 12b, Fig. 13b, Fig. 14b, and Fig. 15b) of each cell: C2C12 (Fig. 12), Hepa1-6 (Fig. 13), L929 (Fig. 14), and Neuro-2a (Fig. 15), respectively. In these figures, each mark of circle and of triangle shows datum before the slit and in the slit, respectively. Data are arranged in the ascending order of the projected area before the slit (A_1) in Figs. 12a, 13a, 14a and 15a. The datum on each cell is arranged at the corresponding cell number.

The area of every cell increases in the slit, which shows deformation to a flat disk in the slit (Figs. 12a, 13a, 14a, 15a). None of the cell L929 has the projected area smaller than $300 \mu\text{m}^2$ before the slit (A_1) (Fig. 14a). The velocity of L929 is slow in the slit (v_2) (Fig. 14b).

In Fig. 15b, the velocity of Neuro-2a in the slit (v_2 : triangle) tends to decrease with increase of the projected area before slit (A_1). The tendency shows the passing velocity decreases with the own higher deformation ratio of each cell. Both at C2C12 (Fig. 12b) and at Hepa1-6 (Fig. 13b), on the other hand, the velocity in the slit (v_2) scatters, which shows some cells passed through the slit relatively fast with the high deformation ratio. Especially at several cells of C2C12, the velocity in the slit (v_2) is higher than that before the slit (v_1) (Fig. 12b).

The relationship between the velocity ratio (R_v) and the deformation ratio (R_a) is summarized in Fig. 16. Some cells of L929 have the deformation ratio above 1.0, which shows the large deformation of the cell in the slit. Several cells of C2C12 have the velocity ratio above 1.0, which shows accelerated velocity in the slit. The velocity ratio tends to

decrease with the increase of the deformation ratio. In Fig. 16, each line shows the approximate straight line of data belong to each kind of cells. Every line has negative slope. The line of C2C12 has the steepest negative slope. The slope of each line is -3.3 (C2C12), -2.1 (Hepa1-6), -1.7 (L929), and -0.6 (Neuro-2a), respectively.

4. DISCUSSION

For the reason of the limitation of the photolithography process, the edge of the ridge is not sharp, but it has the edge with the small width. The biological system might have the sharper edge, so that a cell passes easily through the slit with the shorter travel distance *in vivo* [5]. The cell has to struggle to pass through the slit in the present experimental device with the longer travel distance.

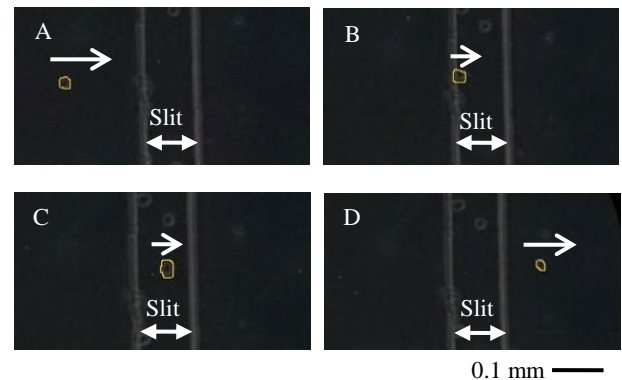


Fig. 11: Cell (traced by yellow line) approaches to slit (A), enters into slit (B), is passing through slit (C), and leaves from slit (D): flow from left to right.

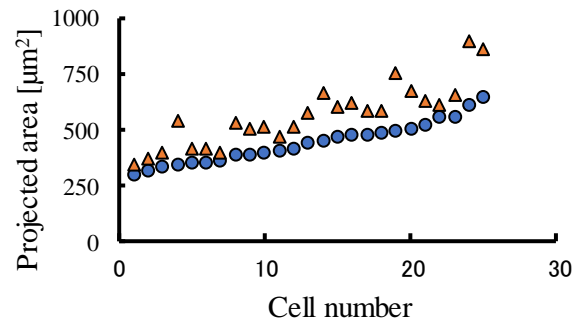


Fig. 12a: Area of C2C12: before slit (circle), in slit (triangle).

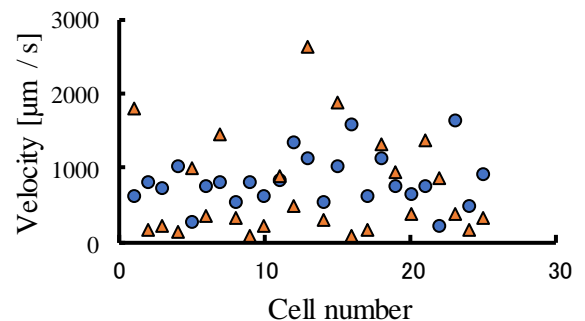


Fig. 12b: Velocity of C2C12: before slit (circle), in slit (triangle).

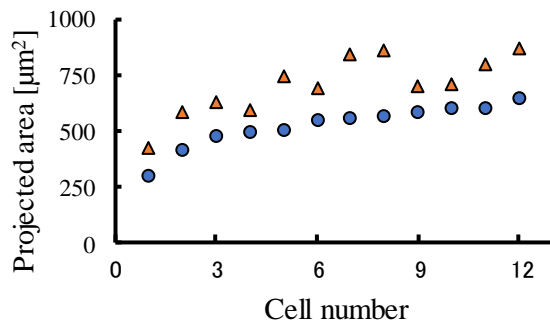


Fig. 13a: Area of Hepa1-6: before slit (circle), in slit (triangle).

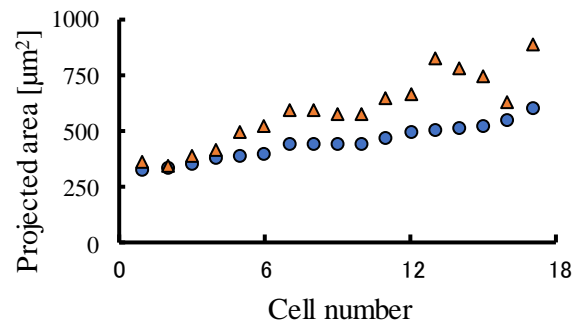


Fig. 15a: Area of Neuro-2a: before slit (circle), in slit (triangle).

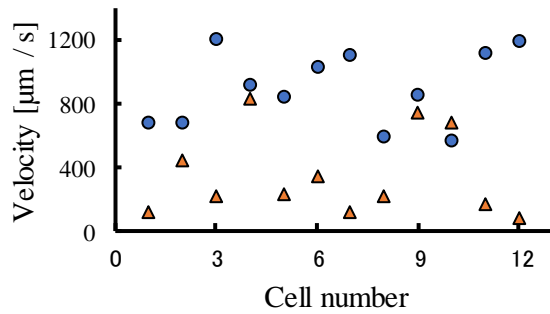


Fig. 13b: Velocity of Hepa1-6: before slit (circle), in slit (triangle).

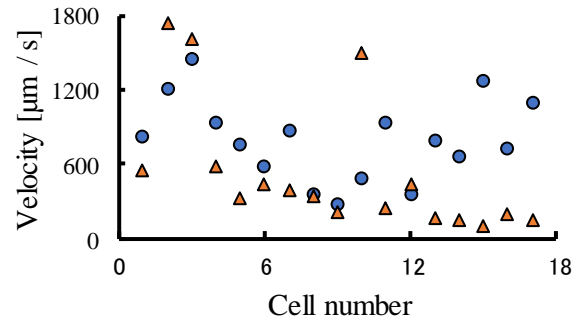


Fig. 15b: Velocity of Neuro-2a: before slit (circle), in slit (triangle).

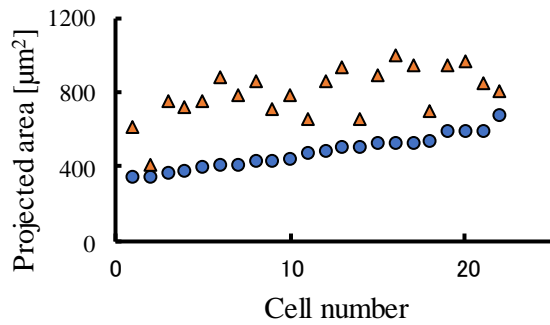


Fig. 14a: Area of L929: before slit (circle), in slit (triangle).

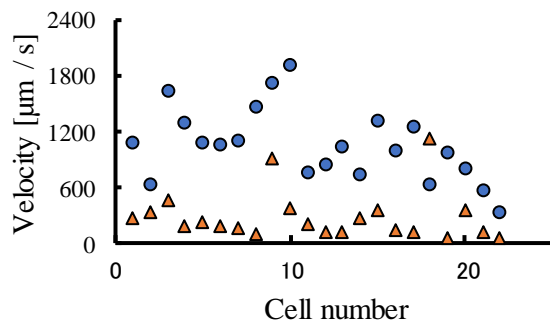


Fig. 14b: Velocity of L929: before slit (circle), in slit (triangle).

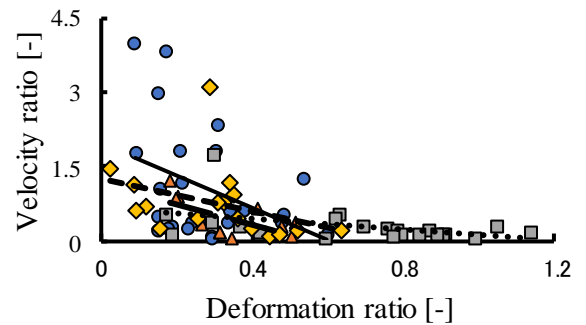


Fig. 16: Relationship between velocity ratio (R_v) and deformation ratio (R_d): C2C12 (circle), Hepa1-6 (triangle), L929 (square), Neuro-2a (rhombus): approximate straight line is added.

The dimension of the slit was confirmed by the passing velocity of porcine red blood cells in the present study. The ratio of the cross-sectional area between the flow channel ($0.06 \text{ mm} \times 2 \text{ mm}$) and the slit ($0.01 \text{ mm} \times 0.8 \text{ mm}$) is 15, so that the mean flow velocity of the media in the slit is 15 times faster than that before the slit. Every datum of the velocity ratio in Fig. 16 is smaller than 5, which depends on the friction between the cell and the wall of the slit.

The moving velocity of the cell suspended in the media follows the media velocity. In the previous study [10], the flow rate was controlled by the syringe pump, but the flow rate varied because of several factors: the compliance of the wall of the flow path, and clogging of the flow path.

The flow rate is controlled by the pressure difference between inlet and outlet of the flow channel in the present study, which has advantage to keep the inner pressure of the flow channel for the morphological stability of the flow channel. The moving velocity also depends on the interaction between the cell and the surface of the slit (friction). To keep the surface property of the channel stable, bovine serum albumin is pre-coated on the surface of the flow path by prefilling the bovine serum albumin solution in the channel in the present study. The sphere with the diameter of 18 μm makes the projected circle area of 250 μm^2 . Because the projected area is larger than 250 μm^2 in the slit, every cell is forced to be deformed in the slit of 10 μm height in the present study (Figs. 12, 14, 16, and 18). The biological cells are sorted according to the shape, and deformability *in vivo*. Several cells pass through the micro slit. Some cells or fragments, which pass through the slit, are decomposed. Some cells, which cannot pass through the narrow channel, are, on the other hand, captured at the channel. A red blood cell has a high deformability. It deforms from the biconcave disk shape to the parachute like shape, when it is passing through the micro capillary. In the shear field, the red blood cell rotates and deforms to the ellipsoid shape. The most of biological cells, on the other hand, mostly keep the spherical shape, when they are flowing in the medium. The deformability of a red blood cell changes with aging [3]. The deformability of the biological single cell depends on several factors. The deformability has been analyzed in several studies: using microfluidics [9], measuring local viscoelasticity [12], using atomic force microscopy [13, 14], and using cell mechanics model [15]. The methodology can also be applied to the sorting technology on cells [16, 17]. The deformation is evaluated with the ratio of the projected area of the plan view of the disk-like shape during the passing through the slit in the present study. The deformation in the perpendicular direction can be observed at another type of the slit between micro cylindrical pillars [10].

5. CONCLUSION

Deformation of a cell through the slit (0.8 mm width, and 0.01 mm height) between micro-machined (photolithography technique) surfaces has been observed *in vitro*. Both the projected area and the passing velocity in the slit have been evaluated at the microscopic images. The passing velocity of each cell tends to decrease with the higher deformation ratio. The tendency depends on cell types. Some cells of C2C12 (mouse myoblast cells) and of Hepa1-6 (mouse hepatoma cells) pass through the slit relatively fast at the higher deformation ratio. At some cells of C2C12, the velocity in the slit is higher than that before the slit. The designed slit between micro-machined surfaces has capability to sort cells according to their deformability.

REFERENCES

- [1] J. Sleep, D. Wilson, R. Simmons, and W. Gratzner, "Elasticity of the Red Cell Membrane and Its Relation to Hemolytic Disorders: An Optical Tweezers Study", **Biophysical Journal**, Vol. 77, No. 6, 1999, pp. 3085–3095.
- [2] S. Sakuma, K. Kuroda, C.-H.D. Tsai, W. Fukui, F. Arai and M. Kaneko, "Red Blood Cell Fatigue Evaluation Based on the Close-encountering Point between Extensibility and Recoverability", **Lab on a Chip**, Vol. 14, 2014, pp. 1135–1141.
- [3] S. Hashimoto, H. Otani, H. Imamura, et al., "Effect of Aging on Deformability of Erythrocytes in Shear Flow", **Journal of Systemics Cybernetics and Informatics**, Vol. 3, No. 1, 2005, pp. 90–93.
- [4] S. Hashimoto, "Detect of Sublethal Damage with Cyclic Deformation of Erythrocyte in Shear Flow", **Journal of Systemics Cybernetics and Informatics**, Vol. 12, No. 3, 2014, pp. 41–46.
- [5] L.T. Chen and L. Weiss, "The Role of the Sinus Wall in the Passage of Erythrocytes through the Spleen", **Blood**, Vol. 41, No. 4, 1973, pp. 529–537.
- [6] Y. Takahashi, S. Hashimoto, H. Hino, A. Mizoi and N. Noguchi, "Micro Groove for Trapping of Flowing Cell", **Journal of Systemics, Cybernetics and Informatics**, Vol. 13, No. 3, 2015, pp. 1–8.
- [7] S. Hou, H. Zhao, L. Zhao, Q. Shen, K.S. Wei, D.Y. Suh, A. Nakao, M.A. Garcia, M. Song, T. Lee, B. Xiong, S.C. Luo, H.R. Tseng and H.H. Yu, "Capture and Stimulated Release of Circulating Tumor Cells on Polymer-Grafted Silicon Nanostructures", **Advanced Materials**, Vol. 25, No. 11, 2013, pp. 1547–1551.
- [8] L.M. Lee and A.P. Liu, "A Microfluidic Pipette Array for Mechanophenotyping of Cancer Cells and Mechanical Gating of Mechanosensitive Channels", **Lab on a Chip**, Vol. 15, 2015, pp. 264–273.
- [9] H.W. Hou, Q.S. Li, G.Y.H. Lee, A.P. Kumar, C.N. Ong and C.T. Lim, "Deformability Study of Breast Cancer Cells Using Microfluidics", **Biomedical Microdevices**, Vol. 11, No. 3, 2009, pp. 557–564.
- [10] Y. Takahashi, S. Hashimoto, H. Hino and T. Azuma, "Design of Slit between Micro Cylindrical Pillars for Cell Sorting", **Journal of Systemics, Cybernetics and Informatics**, Vol. 14, No. 6, 2016, pp. 8–14.
- [11] Y. Takahashi, S. Hashimoto, A. Mizoi and H. Hino, "Deformation of Cell Passing through Micro Slit between Micro Ridges Fabricated by Photolithography Technique", **Journal of Systemics, Cybernetics and Informatics**, Vol. 15, No. 3, 2017, pp. 1–9.
- [12] A.R. Bausch, W. Moeller and E. Sackmann, "Measurement of Local Viscoelasticity and Forces in Living Cells by Magnetic Tweezers", **Biophysical Journal**, Vol. 76, No. 1, 1999, pp. 573–579.
- [13] E. A-Hassan, W.F. Heinz, M.D. Antonik, N.P. D'Costa, S. Nageswaran, C.-A. Schoenenberger and J.H. Hoh, "Relative Microelastic Mapping of Living Cells by Atomic Force Microscopy", **Biophysical Journal**, Vol. 74, No. 3, 1998, pp.1564–1578.
- [14] S.E Cross, Y.-S. Jin, J. Tondre, R. Wong, J.Y. Rao and J.K. Gimzewski, "AFM-based Analysis of Human Metastatic Cancer Cells", **Nanotechnology**, Vol. 19, No. 38, 2008, 384003, pp.1–8.
- [15] G. Bao and S. Suresh, "Cell and Molecular Mechanics of Biological Materials", **Nature Materials**, Vol. 2, No. 11, 2003, pp. 715–725.
- [16] B. Lincoln, H.M. Erickson, S. Schinkinger, F. Wottawah, D. Mitchell, S. Ulvick, C. Bilby and J. Guck, "Deformability-Based Flow Cytometry", **Cytometry**, Part A: the journal of the International Society for Analytical Cytology, Vol. 59, No.2, 2004, pp. 203–209.
- [17] Y. Takahashi, S. Hashimoto and M. Watanabe, "Dielectrophoretic Movement of Cell around Surface Electrodes in Flow Channel", **Journal of Systemics Cybernetics and Informatics**, Vol. 16, No. 3, 2018, pp. 81–87.

